retical bending efficiency is also shown in Fig. 3B. The peaks in Fig. 3B confirm a subtle and important point about PBG waveguides. Indeed, the detection of light at the end of a straight waveguide would not be a sufficient condition, in itself, to confirm PBG guiding. It is the existence of transmission peaks around the sharp bend, along with the specific position of these peaks, that validates the model.

The position of the peaks can be predicted with a 1D scattering theory (*5*). The <11> bending section is modeled as a scattering center with a channel length L (Fig. 4). Light propagating along the <10> direction is scattered by the <11> section into the <01> direction. We label the wave vectors associated with the <10>, <11>, and <01> states as $\mathbf{k}_1(f)$, $\mathbf{k}_2(f)$, and $\mathbf{k}_1(f)$, respectively. The strength of the scattering is determined by the mismatch between $\mathbf{k}_1$ and $\mathbf{k}_2$. If the mismatch is small [the dispersion $\mathbf{k}(f)$ is close to being isotropic], forward scattering is favored, and high transmission efficiency is expected. Complete forward scattering occurs when a resonance inside the bend is established. At such a resonance, light travels freely through the bend with 100% efficiency.

Quantitatively, the reflection coefficient near the transmission peaks is given by $R(f) \cong 4 \times (\Delta\mathbf{k}/\mathbf{k})^2 \times [\sin(\mathbf{k}_2 L)]^2$, where $\Delta\mathbf{k} = (\mathbf{k}_1 - \mathbf{k}_2)/2$ is the wave vector mismatch and $\mathbf{k} = (\mathbf{k}_1 + \mathbf{k}_2)/2$ is the average wave vector. Resonance occurs when $\sin[(\mathbf{k}_2 (f)\mathrm{L}] = 0$. The position of the transmission peaks can readily be obtained by computing the dispersion relation $\mathbf{k}_2(f)$ and by determining the length of the <11> waveguide section. For the bending geometry shown in the inset of Fig. 3B, we found $f_1 = 87.5$ GHz and $f_2 = 101$ GHz. To further test the 1D scattering theory, we also carried out measurements for different bending geometries with $L = 1.33 \times \sqrt{2}a$ and $L = 3.33 \times \sqrt{2}a$. The measured and computed peaks are given in Table 1. The agreement between experiment and theory is excellent confirmation of the validity of the 1D model, hence confirming the existence of guided modes in the photonic crystal.

The 1D model also predicts high transmission efficiency in PBG waveguides with zero radius of curvature. A schematic of the bending geometry is shown in Fig. 3C along with the experimental data. As predicted, the transmission spectrum does not display a series of peaks, yet it shows an overall transmission efficiency larger than 80%. This high transmission efficiency can be compared with ~30% transmission efficiency in similar high-index dielectric waveguides (*5*).

References and Notes

1. See, for example, C. Yeh, *Applied Photonics* (Academic Press, San Diego, CA, 1994).
2. C. Wu, *Science News* **150**, 309 (1996); G. Taubes, *Science* **278**, 1709 (1997).
3. E. A. J. Marcatili, *Bell Syst. Tech. J.* **48**, 2103 (1969).
4. J. D. Joannopoulos, R. D. Meade, J. N. Winn, *Photonic Crystals* (Princeton Univ. Press, New York, 1995).
5. A. Mekis *et al.*, *Phys. Rev. Lett.* **77**, 3787 (1996).
6. M. M. Sigalas *et al.*, in *Proceedings of the 14th Annual Review of Progress in Applied Computational Electromagnetics* (Applied Computational Electromagnetics Society, Monterey, CA), pp. 144–150.
7. J. D. Joannopoulos, P. R. Villeneuve, S. Fan, *Nature* **386**, 143 (1997).
8. E. Yablonovitch and T. J. Gmitter, *Phys. Rev. Lett.* **63**, 1950 (1989); K. M. Ho, C. T. Chan, C. M. Soukoulis, *ibid.* **65**, 3152 (1990); K. M. Leung and Y. F. Liu, *ibid.*, p. 2646; H. S. Sozuer and J. W. Haus, *J. Opt. Soc. Am. B* **10**, 296 (1993).
9. S. Y. Lin and G. Arjavalingam, *Opt. Lett.* **18**, 1666 (1993).
10. J. C. Chen and K. Li, *Microwave Opt. Technol. Lett.* **10**, 319 (1995).
11. To the best of our knowledge, even for a metallic millimeter-wave 90° waveguide bend, the best commercially available one has a bending radii of 4 to 5 wavelengths.
12. Our measurement is accurate to about ±5% mainly because of an amplitude oscillation caused by resonance between the input and output end of the PBG guide. Also, the absolute bending efficiency is slightly lower, ~3%, because the <10> and <01> sections of the bend would contribute to a small guiding loss.

13. The work at Sandia National Laboratories is supported through the U.S. Department of Energy under contract DE-AC04-94AL85000. Sandia is a multiprogram laboratory operated by Sandia Corporation, a Lockheed Martin Company, for the U.S. Department of Energy. The work at Massachusetts Institute of Technology is supported in part by the Material Research Science and Engineering Center program of the NSF under award DMR-9400334.

6 July 1998; accepted 10 September 1998

Organic Carbon Fluxes and Ecological Recovery from the Cretaceous-Tertiary Mass Extinction

Steven D'Hondt, Percy Donaghay, James C. Zachos, Danielle Luttenberg, Matthias Lindinger

Differences between the carbon isotopic values of carbonates secreted by planktic and benthic organisms did not recover to stable preextinction levels for more than 3 million years after the Cretaceous-Tertiary mass extinction. These decreased differences may have resulted from a smaller proportion of marine biological production sinking to deep water in the postextinction ocean. Under this hypothesis, marine production may have recovered shortly after the mass extinction, but the structure of the open-ocean ecosystem did not fully recover for more than 3 million years.

A wide range of geochemical evidence indicates that the organic flux from the surface ocean to the deep sea decreased drastically at the time of the Cretaceous-Tertiary (K-T) mass extinction and did not recover for more than a million years. The evidence for this collapse of the deep-sea organic flux includes dramatic decreases in (i) carbon isotopic ($\delta^{13}C$) differences between carbonate skeletons secreted by planktic and benthic organisms (usually foraminifera) (*1–6*), (ii) $\delta^{13}C$ differences between benthic foraminiferal skeletons (tests) from different ocean basins (*2*), (iii) $\delta^{13}C$ differences between the tests of benthic foraminifera that lived on the seafloor and those that lived in the underlying sediment (*3*), and (iv) the accumulation of barium in deep-sea sediments (*3*).

Our study of planktic-to-benthic $\delta^{13}C$ differences indicates that final recovery of the organic flux to the deep sea may have occurred more than 3 million years after the mass extinction (Figs. 1 and 2). An early phase of recovery is marked by the return of planktic-to-benthic $\delta^{13}C$ differences (and interbenthic $\delta^{13}C$ differences) to low but relatively stable levels within the first several hundred thousand years after the extinction (*1–4*). This early stage of recovery has been identified at Pacific, Southern Ocean, and South Atlantic sites (*1–4*). After this early phase of recovery, differences between planktic and benthic $\delta^{13}C$ values at South Atlantic Deep Sea Drilling Project (DSDP) site 528 remained below preextinction levels for more than 2 million additional years (Fig. 2). At site 528, the final recovery of planktic-to-benthic $\delta^{13}C$ differences is exhibited by fine (<25 μm in diameter) $CaCO_3$, near-surface planktic foraminifera and planktic foraminifera that lived deeper in the thermocline (*7*) (Fig. 2). The parallel nature of these planktic-to-benthic records provides strong evidence that surface-to-deep $\delta^{13}C$ gradients did not fully recover for more than 3 million years after the

S. D'Hondt, P. Donaghay, D. Luttenberg, Graduate School of Oceanography, University of Rhode Island, Narragansett, RI 02882, USA. J. C. Zachos, Earth Sciences Department, University of California, Santa Cruz, CA 95064, USA. M. Lindinger, Rossinistrasse 5, D-88353 Kissligg, Germany.

mass extinction. Data from Central Pacific DSDP site 577 indicate that this long delay in final recovery was global (Fig. 3).

A low-productivity "Strangelove" ocean has often been invoked to explain a low organic flux to the deep sea during the earliest Tertiary (*1–3*, *8*). A low-productivity ocean would naturally have occurred during any interval of darkness that resulted from the K-T impact of a large asteroid or comet. However, global darkness would have lasted only a few years (*9*). Because phytoplankton typically double on time scales of hours to days (*10*), it would have been difficult to maintain a low-productivity ocean once surface irradiance recovered.

We propose that once sunlight returned, biological productivity also returned, but planktic-to-benthic $\delta^{13}C$ differences remained low because a smaller fraction of marine production sank to deep waters in the postextinction ocean. Such a reduction in the organic flux to deep waters could have been a natural consequence of the ecosystem reorganization that resulted from the mass extinction, because a general absence of large pelagic grazers or a decrease in the mean size of phytoplankton would have greatly reduced the packaging of biomass into the large particles that sink to the deep ocean. Application of this hypothesis to our data implies that final recovery of the open-ocean ecosystem structure occurred more than 3 million years after the mass extinction (*11*). Such recovery may have required the evolution of new species at multiple trophic levels to replace those lost during the mass extinction.

Total organic production in the modern open ocean is between 30×10^{15} and 50×10^{15} g of carbon per year (*12, 13*). Most of this carbon is oxidized in relatively shallow waters; only about 10% sinks to a water depth of 200 m, and only 1% actually reaches deep-sea sediments (*12*). Most of the organic carbon in surface sediments is oxidized by biological activity. Only about 0.3% of open-ocean production is eventually buried in deep-sea sediments (*12*).

For the Strangelove model to explain postextinction maintenance of the mean surface-to-deep $\delta^{13}C$ gradient at 50% of its preextinction level, earliest Tertiary marine biomass production must have been 50% lower than latest Cretaceous production—and the ratio of total production to downward organic flux must have been constant. In contrast, our model allows postextinction production to approximate preextinction production and explains the low postextinction $\delta^{13}C$ gradient by just slightly increasing (from 90 to 95%) the fraction of total production that was degraded in the upper 200 m of the ocean.

The proportion of organic production that sinks from the surface ocean is primarily controlled by the ratio of phytoplanktic respiration to photosynthesis, the size of the phytoplankton that define the base of the

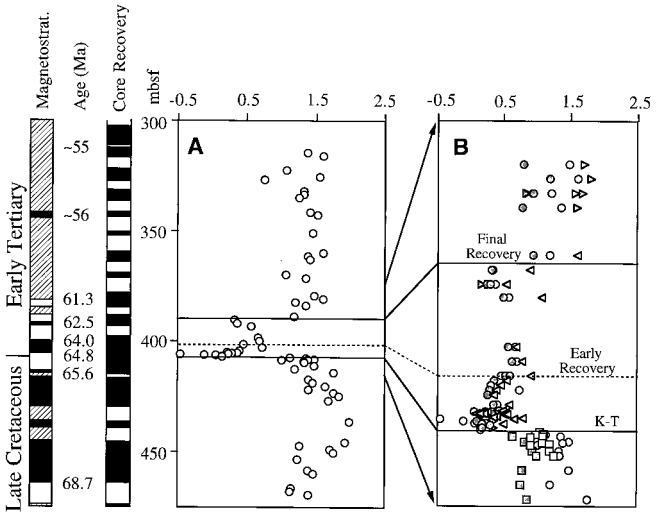

Fig. 1. Cretaceous-Tertiary $\delta^{13}C$ records from South Atlantic DSDP site 528. Magnetostrat., magnetostratigraphy; Ma, million years ago; mbsf, meters below sea floor. (**A**) $\delta^{13}C$ records of benthic foraminifera (*Gavelinella* and *Nuttallides*) (solid circles) and fine (<25 μm) carbonate (open circles) (*23*). (**B**) $\delta^{13}C$ records of benthic foraminifera (solid circles), fine (<25 μm) carbonate (open circles), and planktic foraminifera. Open symbols represent near-surface planktic foraminifera: *Morozovella angulata* (right-pointing open triangles), *Praemurica taurica* (left-pointing open triangles), and *Rugoglobigerina rotundata* (open squares). Gray symbols represent deeper-dwelling planktic foraminifera: *Eoglobigerina eobulloides* (gray circles), *Parasubbotina pseudobulloides* (right-pointing gray triangles), and *Pseudotextularia ultimatumida* (gray squares). Hatched areas represent intervals with insufficient data to assign magnetic polarity. White "core recovery" intervals mark missing sections.

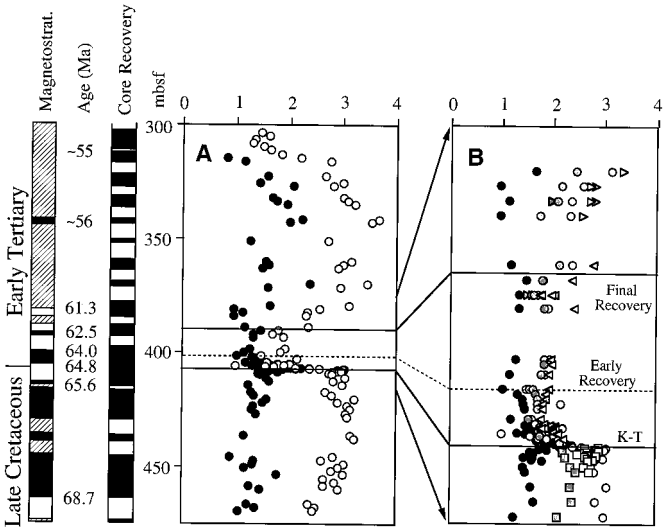

Fig. 2. Cretaceous-Tertiary $\delta^{13}C$ records from site 528 (*23*, *24*). (**A**) $\delta^{13}C$ differences between fine carbonate and benthic foraminifera. (**B**) $\delta^{13}C$ differences between planktic and benthic foraminifera and between fine carbonate and benthic foraminifera. These differences are identified by symbols corresponding to those representing the planktic taxa of Fig. 1.

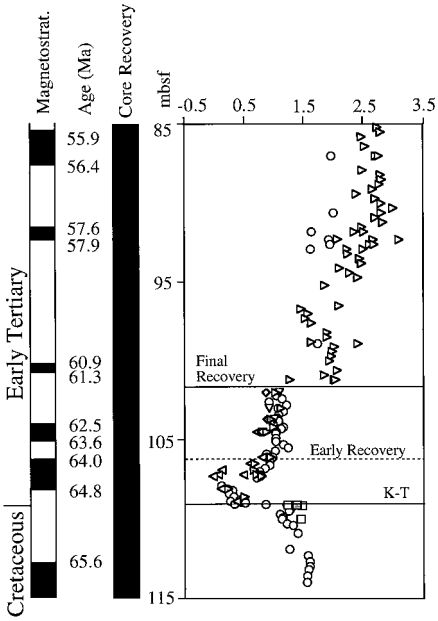

Fig. 3. Cretaceous-Tertiary $\delta^{13}C$ records from DSDP site 577 (*25*). Open circles represent $\delta^{13}C$ differences between bulk carbonate and benthic foraminifera (*Nuttalides*). Other symbols represent differences between planktic and benthic foraminifera. The planktic foraminifera are as follows: *Morozovella* species (right-pointing open triangles), *Praemurica uncinata* (downward-pointing open triangles), *Praemurica taurica* (left-pointing open triangles), *Rugoglobigerina rotundata* (open squares), *Parasubbotina pseudobulloides* (right-pointing gray triangles), *Subbotina triloculinoides* (gray diamonds), and *Pseudotextularia ultimatumida* (gray squares). For further information, see Fig. 1 caption.

trophic structure (small plankton sink too slowly and are degraded too quickly to settle to deep waters), the ability of phytoplankton to aggregate into larger particles, and the size and trophic efficiency of the animals that repackage biomass into larger aggregates that can sink more rapidly (*14*).

An ocean characterized by high rates of picoplankton production (phytoplankton with a diameter less than 2 μm) or low abundances of relatively large grazers (such as macrozooplankton and fish) would be characterized by low rates of biomass sinking to deep waters and high rates of biomass recycling in the upper water column (*15*). In such an ocean, an increased fraction of total production would be shunted through the microbial food web. By allowing essential nutrients to remain in easily remineralized forms (such as tiny microbially grazed plankton) in the euphotic zone, such changes may also increase rates of nutrient recycing and open-ocean biomass production.

The K-T mass extinction radically altered the open-ocean ecosystem. Most species of planktic foraminifera and calcareous nannoplankton went extinct at that time (*16*, *17*). The mean accumulation of calcareous nannofossils in deep-sea sediments decreased by up to 85% (*17*). This decrease in nannofossil accumulation resulted from an equivalent drop in the production of calcite-secreting phytoplankton (*17*). The collapse of higher trophic levels is suggested by the fossil record of larger organisms. Ammonites (shelled nektonic cephalopods) suffered complete extinction (*18*), as did mosasaurs and sauropterygians (plesiosaurs and pliosaurs) (*19*). Marine osteichthyans (bony fish) and selachians (sharks and rays) underwent tremendous extinction (*19*).

Despite radical K-T changes in the open-ocean ecosystem, at least two lines of evidence suggest that biological production was relatively high during the 3-million-year interval of reduced $\delta^{13}C$ differences. First, despite the mass extinction of planktic foraminifera and a drastic decrease in the test size of planktic foraminifera at the K-T boundary, the mean flux of foraminiferal tests to deep-sea sediments remained relatively stable across the K-T boundary and throughout the earliest Tertiary (*17*). Tiny (<100 μm in diameter) foraminiferal tests are abundant in sediments immediately above the extinction horizon. High concentrations of radiolarian tests and diatom frustules are seen in postextinction marine sediments of New Zealand (*20*). These findings suggest that within a few thousand years of the mass extinction, marine biological production returned to high enough levels to support abundant small zooplankton.

Second, planktic and benthic $\delta^{13}C$ values stabilized within a few hundred thousand years after the K-T extinction (*1–4*) (Fig. 1). Their failure to continue shifting to more negative values suggests that the burial of organic matter recovered to as much as 90% of its preextinction rate (*21*). Final recovery of planktic $\delta^{13}C$ values approximately coincided with the final recovery of planktic-to-benthic $\delta^{13}C$ differences (Figs. 1 and 2). This coincidence suggests that the final recovery of organic burial may have been closely coupled to the final recovery of the organic flux to deep waters.

The sequential recovery of carbon burial and planktic-to-benthic $\delta^{13}C$ differences is consistent with the idea that organic flux to shallow sediments recovered long before the recovery of the organic flux to the deep ocean. This staged recovery of the vertical organic flux is in turn consistent with progressive recovery of open-ocean trophic structures. For example, if abundant grazers became progressively larger over time, the sinking of organic carbon to shallow sediments and water depths of a couple hundred meters would have recovered before the sinking of organic carbon to greater water depths.

Because the organic flux to the deep sea is a major sink for atmospheric CO_2 and biologically limiting nutrients from the surface ocean, the long delay in recovery of planktic-to-benthic $\delta^{13}C$ differences suggests that the global biogeochemical cycles of carbon and other biologically active elements were also altered for up to 3 million years by the pattern of K-T mass extinction and biological recovery. The long-lived $\delta^{13}C$ anomaly associated with the Permo-Triassic mass extinction (*22*) may have similarly resulted from the cycling of carbon by the altered ecosystem of a postextinction ocean.

References and Notes

1. K. J. Hsü *et al*., *Science* **216**, 249 (1982); J. C. Zachos and M. A. Arthur, *Paleoceanography* **1**, 5 (1986); L. D. Stott and J. P. Kennett, *Nature* **342**, 526 (1989).
2. L. D. Stott and J. P. Kennett, *Sci. Res. Ocean Drill. Prog.* **113**, 829 (1990); J. C. Zachos, M.-P. Aubry, W. A. Berggren, T. Ehrendorfer, F. Heider, *ibid*. **120** (part 2), 961 (1992).
3. J. C. Zachos, M. A. Arthur, W. E. Dean, *Nature* **337**, 61 (1989).
4. S. D'Hondt and M. Lindinger, *Lunar Planet. Inst. Contrib.* **673**, 40 (1988); G. Keller and M. Lindinger, *Palaeogeogr. Palaeoclimatol. Palaeoecol.* **73**, 243 (1989); E. Barrera and G. Keller, *Paleoceanography* **5**, 867 (1990); R. M. Corfield, *Earth Sci. Rev.* **37**, 225 (1994).
5. The ratio of ^{13}C to ^{12}C is reported in per mil (‰) notation with respect to the Pee Dee Belemnite standard: $\delta^{13}C = (^{13}C/^{12}C_{sample}/^{13}C/^{12}C_{PDB} - 1) \times 1000$. Carbon-12 is preferentially taken up and incorporated by photosynthetic organisms, causing the average $\delta^{13}C$ of marine organic carbon to differ by about –20 ‰ from the $\delta^{13}C$ of total dissolved CO_2 ($TCO_2 = CO_2 + HCO_3^- + CO_3^-$) in seawater. The sinking and deep-water oxidation of organic carbon preferentially transfer ^{12}C from the surface ocean and atmosphere to the deep ocean, sustaining a modern mean $\delta^{13}C$ difference of about 1.5 ‰ between TCO_2 in surface waters and that in deep waters [T. F. Anderson and M. A. Arthur, in *Stable Isotopes in Sedimentary Geology*, M. A. Arthur *et al.*, Eds. (SEPM Short Course No. 10, Society of Economic Paleontologists and Minerologists, Tulsa, OK, 1983), pp. 1-1-1–151]. Past changes in the $\delta^{13}C$ of TCO_2 in surface and deep waters are respectively tracked by changes in the $\delta^{13}C$ of $CaCO_3$ secreted by surface-water plankton and changes in the $\delta^{13}C$ of $CaCO_3$ secreted by foraminifera that live on the sediment surface. The $\delta^{13}C$ of adult specimens from some modern planktic species can be offset from the $\delta^{13}C$ of their surrounding TCO_2 by as much as 1 ‰ [H. J. Spero and D. W. Lea, *Mar. Micropaleontol.* **22**, 193 (1993)]. However, relatively constant offsets between the $\delta^{13}C$ of dissolved TCO_2 and that of individual foraminiferal species [N. J. Shackleton, M. A. Hall, J. Line, C. Shuxi, *Nature* **306**, 319 (1983); H. J. Spero and D. W. Lea, *Mar. Micropaleontol.* **28**, 231 (1996)] allow the direction of past changes in surface-to-deep $\delta^{13}C$ gradients to be identified.
6. The presence or absence of the drastic K-T decrease in planktic-to-benthic $\delta^{13}C$ differences does not depend on the planktic and benthic species examined (although its magnitude does) (*1–4*). Hence, the reduction in these differences appears to document a real decrease in the $\delta^{13}C$ gradient between TCO_2 in the surface ocean and that in the deep ocean. The latter decrease in turn indicates that much less organic carbon was oxidized in the deep sea after the K-T mass extinction.
7. The planktic-to-benthic $\delta^{13}C$ differences defined by postrecovery *Morozovella* species are even higher than those defined by preextinction *Rugoglobigerina rotundata* (Fig. 2B). It is likely that the relatively high values of *Morozovella* species resulted in part from photosymbiotic stripping of ^{12}C from the HCO_3^- used for calcification [S. D'Hondt, J. C. Zachos, G. Schultz, *Paleobiology* **20**, 391 (1994)]. In contrast, preextinction *Rugoglobigerina* species were asymbiotic (S. D'Hondt and J. C. Zachos, *ibid*., in press) and would not have had photosymbiotically enhanced $\delta^{13}C$ values. Despite *Morozovella* photosymbiosis, the final recovery of planktic-to-benthic $\delta^{13}C$ differences cannot simply be attributed to the evolution of foraminiferal photosymbiosis, because the final $\delta^{13}C$ recovery is exhibited at site 528 by asymbiotic deeper dwelling foraminifera (*Eoglobigerina eobulloides* and *Parasubbotina pseudobulloides*), the asymbiotic ancestor of *Morozovella* (*Praemurica taurica*), and fine (<25 μm) carbonate {which is typically dominated by phytoplanktic nannofossils [C. K. Paull and H. R. Thierstein, *Paleoceanography* **2**, 423 (1987)]}.
8. K. J. Hsü and J. A. McKenzie, *Am. Geophys. Union Geophys. Monogr.* **32**, 251 (1985).
9. K. O. Pope, K. H. Baines, A. C. Ocampo, B. A. Ivanov, *J. Geophys. Res.* **102** (E9), 21645 (1997).
10. L. E. Brand, in *Coccolithophores*, A. Winter and W. G. Siesser, Eds. (Cambridge Univ. Press, Cambridge, 1994), pp. 39–49; F. J. R. Taylor, in *The Biology of Dinoflagellates*, F. J. R. Taylor, Ed. (Blackwell Scientific, Oxford, 1987), pp. 399–502.
11. S. D'Hondt and P. Donaghay, *Geol. Soc. Am. Ann. Meet. Abstr. Prog.* **27**, A164 (1995).
12. W. H. Berger, V. S. Smetecek, G. Wefer, in *Productivity of the Ocean: Present and Past*, W. H. Berger, V.S. Smetecek, G. Wefer, Eds. (Wiley, New York, 1989), pp. 49–63.
13. W. H. Schlesinger, *Biogeochemistry, an Analysis of Global Change* (Academic Press, London, ed. 2, 1997).
14. A. F. Michaels and M. W. Silver, *Deep-Sea Res.* **35**, 473 (1988).
15. Picoplankton produce 30 to 60% of the organic particles in the modern open ocean [M. V. Angel, in *Productivity of the Ocean: Present and Past*, W. H. Berger, V. S. Smetecek, G. Wefer, Eds. (Wiley, New York, 1989), pp. 155–174]. Macrozooplankton cannot effectively graze on picoplankton, which are primarily grazed by small protozoa [T. Fenchel, *Annu. Rev. Ecol. Syst.* **19**, 19 (1988)].
16. J. Smit, *Geol. Soc. Am. Spec. Pap.* **190**, 329 (1982); B. T. Huber, *ibid.* **307**, 319 (1996); J. J. Pospichal, *ibid*., p. 335.
17. S. D'Hondt, T. D. Herbert, J. King, C. Gibson, *ibid.*, p. 303.
18. C. R. Marshall and P. D. Ward, *Science* **274**, 1360 (1996).
19. E. Buffetaut, *Tectonophysics* **171**, 337 (1990).
20. C. J. Hollis, K. A. Rodgers, R. J. Parker, *Geology* **23**, 835 (1995).
21. L. R. Kump, *ibid.* **19**, 299 (1991).
22. W. T. Holser *et al*., *Nature* **337**, 39 (1989); A. Baud, M. Magaritz, W. T. Holser, *Geol. Rundsch.*, **78**, 649 (1989); S. A. Bowring *et al*., *Science* **280**, 1039 (1998).
23. Isotopic data for fine carbonate and benthic foraminifera were generated at Eidgenössische Technische

Hochschule–Zürich according to procedures in S. D'Hondt and M. Lindinger, *Palaeogeogr. Palaeoclimatol. Palaeoecol.* **112**, 363 (1994). Magnetostratigraphy is from A. D. Chave [*Init. Rep. Deep Sea Drill. Proj.* **74**, 525 (1984)]. Age estimates were based on the magnetic polarity time scale of S. C. Cande and D. V. Kent [*J. Geophys. Res.* **100**, 6093 (1995)].

24. Isotopic data for most planktic foraminiferal samples and several benthic samples were generated at the University of California, Santa Cruz, stable isotope laboratory. For planktic samples, we relied on narrowly constrained (one-quarter phi) size fractions of individual species (*Praemurica taurica* and *R. rotundata* were 212 to 250 μm in mean diameter, *P. ultimatumida* was 250 to 300 μm in mean diameter, and all other planktic taxa were 150 to 180 μm in diameter). In preparation for analysis, samples were roasted at 380°C under vacuum for 1 hour. Isotopic analyses were performed with an Autocarb Preparation Device coupled to a Fisons Prism Mass Spectrometer. In this system, each sample is reacted with H_3PO_4 (8 ml) in a common acid bath at 90°C. External analytical precision, based on replicate analyses of two standards, NBS-19 and Carrera Marble, was better than 0.08 and 0.05‰ for O and C isotopes, respectively. Corrections to measured isotope values were made according to H. Craig, *Geochim. Cosmochim. Acta* **12**, 133 (1957). These isotopic data were combined with data from (*23*).
25. *Morozovella* data are from N. J. Shackleton, R. M. Corfield, and M. A. Hall [*J. Foram. Res.* **15**, 321 (1985)] and R .M. Corfield and J. E. Cartlidge [*Terra Nova* **4**, 443 (1992)]. *Nuttalides* data are from (*3*) and K. G. Miller, T. R. Janecek, M. E. Katz, and D. J. Keil [*Paleoceanography* **2**, 741 (1987)]. Several bulk carbonate data are from N. J. Shackleton, M. A. Hall, and U. Bleil [*Init. Rep. Deep Sea Drill. Proj.* **86**, 503 (1985)]. The remaining isotopic data are from (*3*). Because planktic and benthic samples were not consistently paired, many benthic $\delta^{13}C$ estimates were derived by linear interpolation of measured data. The magnetostratigraphy is from U. Bleil, [*Init. Rep. Deep Sea Drill. Proj.* **86**, 441 (1985)]. Age estimates are as in (*23*).
26. This research was supported in part by NSF (Division of Earth Sciences). Samples were provided by the Ocean Drilling Program. The manuscript was improved by the thoughtful comments of two anonymous reviewers.

17 April 1998; accepted 1 September 1998

Climate Change Record in Subsurface Temperatures: A Global Perspective

Henry N. Pollack,* Shaopeng Huang, Po-Yu Shen

Analyses of underground temperature measurements from 358 boreholes in eastern North America, central Europe, southern Africa, and Australia indicate that, in the 20th century, the average surface temperature of Earth has increased by about 0.5°C and that the 20th century has been the warmest of the past five centuries. The subsurface temperatures also indicate that Earth's mean surface temperature has increased by about 1.0°C over the past five centuries. The geothermal data offer an independent confirmation of the unusual character of 20th-century climate that has emerged from recent multiproxy studies.

Temperature changes at Earth's surface propagate slowly downward into the rocks beneath the surface and modify the ambient thermal regime. Thus, present-day subsurface temperatures provide evidence of temperature changes that have occurred at the surface in the past. The information contained in this geothermal archive is a valuable complement to instrumentally acquired temperature data and to various types of temperature proxies for understanding Earth's recent surface temperature history (particularly, for the surface temperature history during the several centuries before the acquisition of an instrumental record). Here we report a five-century surface temperature history that was derived from subsurface temperature observations in 358 boreholes (*1*) in eastern North America, central Europe, southern Africa, and Australia (Fig. 1).

As temperature fluctuations at Earth's surface diffuse downward, their amplitudes diminish exponentially with depth. Shorter period oscillations, such as diurnal and seasonal changes, attenuate more rapidly with depth than do longer period oscillations. Because of this selective filtering, Earth records progressively longer term trends at increasing depths. Thus, the geothermal archive is a natural complement to climate proxies (such as tree rings) that display excellent annual resolution but are more difficult to use in resolving long-term trends.

Typically, borehole temperature measurements are made at 10-m depth intervals with an electrical resistance thermometer that can resolve temperature changes of 0.01°C. Most of the boreholes that we selected for analysis penetrated to depths of 200 to 600 m. In general, all subsurface perturbations arising from surface temperature changes that occurred in the past five centuries are confined to the upper 500 m of Earth's crust.

The reconstruction of surface temperature history from borehole temperatures has drawn increasing attention (*2*) over the past two decades. Most reconstruction techniques involve the process of inversion and therefore must contend with incomplete (finite) and noisy data that make it increasingly difficult to resolve climatic excursions in the more remote past (*3*). Noise in the system is principally of two types: (i) errors in the measurement of temperatures, depths, and thermophysical properties and (ii) errors that arise from departures of the mathematical representation of the system from conditions existing in the real world. Most analyses of borehole climatic perturbations assume that heat is transferred solely through one-dimensional heat conduction. Deviations from this idealization (for example, moving fluids with an associated advective component of heat transfer, lateral heterogeneity in thermal conductivity, and topography and nonuniform vegetation along the surface) are manifest as noise in the analysis (*4*).

In attempting to extract a signal in the presence of noise, one has a number of tools with which to work. Within the process of inversion, there exist various smoothing constraints that can be used to suppress the amplification of noise, but they also mute the signal that is recovered. Smoothing can also be accomplished by the nature of the parameterization of the signal and, in a Bayesian inversion, by the nature of the a priori model. Because individual reconstructions exhibit site-to-site variability (arising from local vegetation, subsurface heterogeneity, and topographic and hydrologic effects) that may mask the regional climatic signal, signal enhancement can also be achieved after inversion by stacking (averaging) a large number of individual results (*5*).

The combination of the predominant depth range of observations and the characteristic magnitude of noise has led us to choose five centuries as the practical interval over which to develop climate reconstructions (*6*). In the parameterization of the surface temperature history, we examine only century-long trends of temperature change. By seeking rates of change, one circumvents the problem of comparing the actual air and ground temperatures. Although the air and ground temperatures are usually not the same, they generally have similar trends (*7*). This sparse parameterization yields estimates of only a few smooth quantities that represent relatively long intervals of time. By estimating century-long parameters, we explicitly designate an adequate averaging interval rather than implicitly incorporate the variable averaging that characterizes the resolution of point estimates (*3*). This simple parameterization also enables one to estimate the total temperature change over the five-century time interval.

In the inversion of individual borehole

H. N. Pollack and S. Huang, Department of Geological Sciences, University of Michigan, Ann Arbor, MI 48109–1063, USA. P.-Y. Shen, Department of Earth Sciences, University of Western Ontario, London, Ontario N6A 5B7, Canada.

*To whom correspondence should be addressed.